Carbon 197 (2022) 18–26

Contents lists available at ScienceDirect

Carbon

journal homepage: www.elsevier.com/locate/carbon

Quantifying the diverse wave effects in thermal transport of nanoporous graphene

Han Wei [a], Yue Hu [a], Hua Bao [a,*], Xiulin Ruan [b,**]

[a] University of Michigan-Shanghai Jiao Tong University Joint Institute, Shanghai Jiao Tong University, Shanghai, 200240, China
[b] School of Mechanical Engineering and Birck Nanotechnology Center, Purdue University, West Lafayette, IN, 47907, USA

ARTICLE INFO

Keywords:
Nanoporous graphene
Thermal conductivity
Wave effect
Thermoelectrics
Quantification

ABSTRACT

Controlling thermal transport in nanoporous graphene through wave-like characteristics of phonons beyond the conventional particle regime has attracted widespread interest. Although the existence of wave-like coherent transport in nanoporous graphene has been proposed, the comprehensive impact on phonon transport remains unclear. In this work, we use a rigorous comparison between non-equilibrium molecular dynamics (NEMD) simulation which captures wave effects and mode-resolved phonon Boltzmann transport equation (BTE) which is a particle approach, to quantify the wave effect contribution in the periodic and aperiodic nanoporous graphene. We find that in periodic nanoporous graphene, the wave effect enhances the thermal conductivity compared to solely particle transport. While in aperiodic nanoporous graphene, we observe the coexistence of diverse wave effects that enhance or reduce thermal transport. The competition of these diverse wave effects can lead to an overall enhancement, decrease, or no impact on the thermal conductivity as compared to the particle transport. Our work reveals insights into wave transport in periodic and aperiodic nanoporous structures and provides important guidance for further tuning the thermal conductivity of nanostructures.

1. Introduction

Graphene, as one of the most important two-dimensional materials, has been widely studied due to its exceptional electronic [1], optical [2], and mechanical [3] properties. In recent years, manipulating the thermal properties of graphene has attracted considerable research interest owing to its applications for thermal management in electronic devices and thermoelectric energy conversion [4–7]. One approach of tailoring the thermal conductivity of graphene is through diffuse phonon scattering by introducing rough surfaces [8–10], impurities [11,12], and defects [13–15], which utilizes particle-like (incoherent) characteristics of phonons. Another approach is through wave interference by introducing secondary artificial periodicities, such as superlattices [16–18], and nanopores [19–22], which is based on wave-like (coherent) characteristics of phonons [23–25].

Nanoporous graphene offers a promising platform for thermoelectrics due to its high tunability of thermal conductivity while maintaining good electrical properties [26]. A good thermoelectric material requires a high electrical conductivity and Seebeck coefficient, and at the same time a low thermal conductivity [27]. The dominant mean free paths of phonons are usually much larger than that of electrons [28]. Properly engineered nanostructures can scatter phonons more effectively than electrons, thereby greatly reducing the thermal conductivity while preserving electrical properties [29,30]. Nanoporous graphene provides such a way to decouple the electron and phonon transport and independently manipulate the thermal conductivity [20,21,31]. Introducing periodic pores is shown to remarkably reduce the thermal conductivity [32–35]. Besides the mass loss and phonon-boundary scattering, coherent transport is generally believed to be another possible reason. It has been theoretically predicted that coherent transport can modify the phonon dispersion relations, thereby giving rise to forbidden bandgap and changing the group velocities and density of states of phonons [25,36]. By introducing the aperiodicity in the pore arrangement, the thermal conductivity of nanoporous graphene was found to be further reduced [19,37]. This is commonly regarded as the result of another behavior of coherent transport, i.e. phonon localization [38–43], which has been directly probed by wave-packet simulations [37,44]. Although it is widely aware of the existence of coherent transport in nanoporous graphene, its contribution to thermal conductivity remains unclear. To better understand the phonon transport mechanism, it is necessary to

* Corresponding author.
** Corresponding author.
E-mail addresses: hua.bao@sjtu.edu.cn (H. Bao), ruan@purdue.edu (X. Ruan).

https://doi.org/10.1016/j.carbon.2022.06.011
Received 5 March 2022; Received in revised form 3 May 2022; Accepted 7 June 2022
Available online 11 June 2022

separate the particle and wave transport and distinguish those diverse wave effects.

There have been several works attempting to separate the particle and wave effect in the thermal transport of nanostructured materials [32,37,45–49]. Hu et al. [37] decomposed the coherent and incoherent phonon transport in nanoporous graphene based on an analytical two-phonon model proposed in Ref. [46]. In this model, phonons are treated as gray-medium and thus the spectral phonon information is neglected [37,46]. Also, the molecular dynamics results were not compared to those from a particle approach [37]. Experimental measurements were compared to particle models to identify the wave effects in nanoporous silicon membranes [45,47], in which the particle models approximated either the phonon dispersion or detailed porous geometries [45,47]. These assumptions lead to the inconsistency of the studied system in the experiments and particle models, making the comparison not on the same footing. Thereafter, a more rigorous approach is needed for decomposing and quantifying wave effect on thermal transport.

In this work, we demonstrate a quantitative study of phonon wave effects in nanoporous graphene. The wave effects are decomposed and discerned by comparing the thermal conductivities computed by mode-resolved phonon Boltzmann transport equation (BTE) and non-equilibrium molecular dynamics (NEMD). The intrinsic phonon properties of graphene and detailed geometries are ensured the same in the two methods. We investigate the wave effect contribution in periodic and aperiodic nanoporous graphene of different geometries. The rest of the manuscript is organized as follows. In Section 2, we introduce the methodology of separating and quantifying wave effect contribution. In Section 3, the thermal conductivities of nanoporous graphene with different periods, system lengths, and degrees of the disorder computed by NEMD and BTE are presented. The wave effect contributions are analyzed in detail. In Section 4, we discuss the results. In Section 5, we give a summary and conclusion.

2. Method and simulation setup

In this section, we first introduce the model for nanoporous graphene. We then propose the methodology of decomposing wave effect by comparing the thermal conductivity values computed by NEMD and mode-resolved phonon BTE.

2.1. Model for nanoporous graphene

The schematic of nanoporous graphene is shown in Fig. 1. In this work, we consider periodic and aperiodic configurations with different periods p, and lengths L. For aperiodic configurations, pore arrangements with different degrees of the disorder are also studied. We generate the aperiodic configuration by randomly shifting each pore from the periodic position by integer multiples of the lattice constant (0.14 nm), which ensures that the center of a shifted pore is always located at a lattice point. The degree of disorder along the x and y-direction for an aperiodic configuration is denoted by (δ_x, δ_y). The integer δ_x and δ_y are limited by the period of the configuration. With increasing periods, the maximum values of δ_x and δ_y are larger. Namely, the shift distance of a pore from the periodic position can be larger for a larger period. The details of generating aperiodic structures with an assigned degree of the disorder (δ_x, δ_y) are presented in Section S1 in Supplementary Materials. For all configurations, the porosity is fixed at 0.1.

2.2. Decomposition and quantification of wave effect

To decompose the wave effect, it is necessary to study exactly the same nanoporous structure using two different approaches, one with wave effect and the other with only particle effect. Here we propose a strategy for extracting wave effects in nanoporous graphene by comparing the thermal conductivity values computed by NEMD and mode-resolved phonon BTE with the same intrinsic phonon properties.

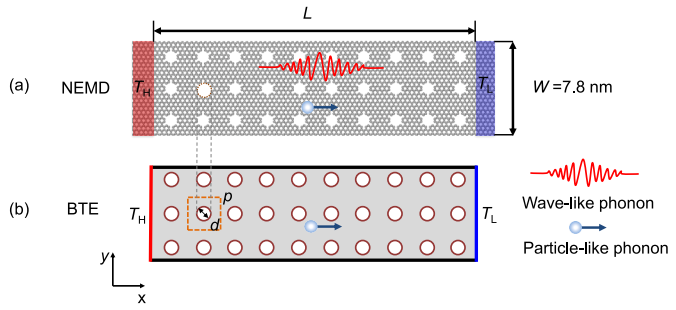

Fig. 1. The schematic of the model for nanoporous graphene and the method of extracting the wave effect from the comparison of NEMD (a) and BTE (b). NEMD includes both wave and particle-like phonon transport, while BTE only considers particle transport. With a proper simulation setup, the wave effect contribution can be extracted from the difference between thermal conductivities predicted by NEMD and BTE. The geometries of nanoporous graphene in NEMD and BTE are kept the same, including the system length L, width W (fixed at 7.8 nm), period p, pore diameter d, porosity (fixed at 0.1), and detailed pore arrangement. In NEMD, atoms at two ends are coupled with a Langevin thermostat at temperature T_H and T_L. Fixed and periodic boundary conditions are adopted along with the length and width directions, respectively. In BTE, the thermalizing boundary condition with T_H and T_L is set for the left and right boundaries, respectively. The top and bottom boundaries are both set as periodic boundaries. The boundary of the pore is set as a diffusely reflecting boundary. In NEMD and BTE, the temperature of T_H and T_L are set at 310 K and 290 K, respectively. (A colour version of this figure can be viewed online.)

The schematic of decomposing wave effect from the comparison of NEMD and BTE is presented in Fig. 1. The detailed geometries of nanoporous graphene, including the system length L, width W (fixed at 7.8 nm), period p, pore diameter d, porosity (fixed at 0.1), and pore arrangement, are identical in NEMD and BTE. NEMD naturally includes wave effect while BTE only considers particle transport. The wave effect is extracted from the difference between thermal conductivities computed by NEMD and BTE. We emphasize that, in order to make a fair quantitative comparison, one needs to ensure that the thermal conductivity obtained by NEMD and BTE quantitatively agree with each other when no wave effect exists. In our recent work, we showed that NEMD and mode-resolved BTE yield quantitatively identical thermal conductivity values for silicon thin films with proper simulation setup [50]. As will be shown later, the thermal conductivity values of NEMD and BTE for pristine graphene without pores can also be identical. Therefore, for nanoporous structures in which the wave effect exists, the difference between NEMD and BTE predicted thermal conductivities can be solely attributed to the wave effect. This approach allows us to separate particle and wave effects of the pores on thermal transport.

In NEMD, the intrinsic phonon properties are naturally determined by the interatomic potentials [50,51], while in mode-resolved phonon BTE [52,53], the intrinsic phonon properties are external input information [52,53]. For steady-state phonon BTE, the input phonon property is the thermal conductivity accumulation distribution with respect to the phonon mean free path (MFP) [54,55], also known as cumulative MFP distribution [56]. We adopt the approach of reconstructing the intrinsic cumulative MFP distribution proposed by Minnich [57]. Through this approach, we ensure the same intrinsic phonon properties in NEMD and BTE. The details are provided in Appendix. To validate the accuracy of the reconstructed MFP distribution, we compare the thermal conductivities at different lengths and corresponding temperature profiles computed by NEMD and mode-resolved BTE with the reconstructed MFP distribution. Fig. 2a shows the thermal conductivities of pristine graphene at different lengths L. It can be seen that the thermal conductivities computed by mode-resolved BTE with reconstructed MFP distribution (gray line) agree well with those computed by NEMD (orange filled circles) at all lengths. They are also consistent with the NEMD results in Ref. [58]. Fig. 2b shows a temperature profile of graphene at

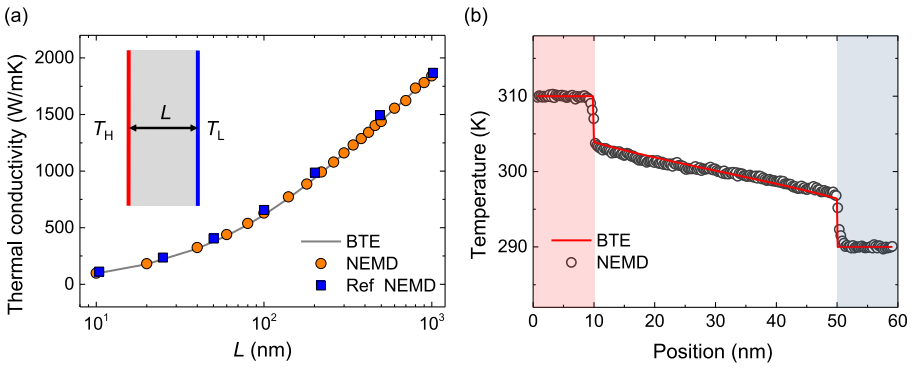

Fig. 2. Comparison between NEMD simulation and mode-resolved phonon BTE calculation with reconstructed MFP distribution for pristine graphene. (a) Thermal conductivities of pristine graphene at different lengths from NEMD simulation (orange filled circles) and BTE calculation (gray line). They are consistent with the NEMD results in Ref. [58] (blue filled squares). (b) The temperature profile of pristine graphene at the length of 40 nm from NEMD simulation (black hollow circles) and BTE calculation (red line). The shaded regions represent the heat source (red) and heat sink (blue), and the region in between represents the sample. (A colour version of this figure can be viewed online.)

the length of 40 nm computed by NEMD (black hollow circles) and BTE (red line), which agree well with each other. These results indicate that for pristine graphene of different lengths, NEMD and BTE are identical. The consistency between NEMD and BTE results is crucial, which allows us to make a meaningful comparison between these two methods when applied to nanoporous graphene to quantify the wave effects.

We define the contribution of the wave effect as

$$\eta_{\text{wave}} = \frac{\kappa_{\text{NEMD}} - \kappa_{\text{BTE}}}{\kappa_{\text{NEMD}}} \times 100\%, \tag{1}$$

where κ_{NEMD} and κ_{BTE} are the thermal conductivity values of nanoporous graphene obtained by NEMD simulation and mode-resolved phonon BTE calculation, respectively. In another perspective, κ_{NEMD} is the "true" value of thermal conductivity and κ_{BTE} is the roughly "estimated" value of thermal conductivity with a certain "error". Correspondingly, η_{wave} can be regarded as the estimation deviation of BTE calculation.

2.3. NEMD simulation and BTE calculation

Here, we introduce the simulation setup of NEMD and mode-resolved phonon BTE. NEMD simulations are performed with the LAMMPS package [59]. Fixed and periodic boundary conditions are adopted along with the length and width directions, respectively. Tersoff potential is used to simulate the interatomic interactions among the carbon atoms [60]. The time step is set as 0.1 fs. Each atomic structure is relaxed through three steps. First, an NVT ensemble with a Langevin thermostat is performed for 0.2 ns (2×10^6 steps) to heat the system to 300 K. Next, an NPT ensemble is performed to release the internal stress for 0.2 ns. Then, an NVT ensemble is applied for another 0.2 ns to further equilibrate the system. After relaxation, 2 layers of atoms at each end are fixed, and the next 38 layers at each end are coupled with a Langevin thermostat at 310 K and 290 K, respectively. We run another 4 ns (4×10^7 steps) to reach a steady-state and then record the temperature distribution and heat current data. The total simulation time is 4.6 ns. The thermal conductivity is computed based on the heat flux and temperature difference $\kappa = -q''/(\Delta T/L)$ [58], where q'' is the heat flux, ΔT is the temperature difference between the heat source and heat sink, and L is the system length. To examine the uncertainty of NEMD simulations, we randomly select typical pristine and nanoporous graphene structures and compute their thermal conductivities with three independent NEMD simulations. It is found that the uncertainties of NEMD of all cases are smaller than 3%. As will be shown later, the uncertainties of NEMD are much smaller than the differences between NEMD and BTE for most nanoporous configurations. Therefore, we believe the result of one NEMD simulation is reliable and we only perform one NEMD simulation for each configuration in this work. The details for uncertainty analysis of NEMD are shown in Section 2 in Supplementary Materials.

The mode-resolved BTE is solved with the finite volume method and the discrete ordinate method with in-house codes. The spatial domain is discretized into unstructured grids. The angular domain at each spatial point is discretized into 12 non-overlapping control angles. The reconstructed cumulative MFP distribution is discretized into 50 bands. The classical distribution for phonons is adopted in BTE calculations and the division of phonon bands. The discretized number of the band, spatial grid, and angles ensure the convergence of results. The thermalizing boundary condition with a temperature of 310 K and 290 K is set for the left and right boundaries, respectively. The top and bottom boundaries are both set as periodic boundaries. The boundary of the pore is set as a diffusely reflecting boundary. Theoretically, it is impossible to set boundary specularity in BTE that is completely equivalent to NEMD, because the concept of "phonon boundary scattering" is already based on the particle transport picture. There is probably no rigorous correspondence with phonon transport in the nanoporous materials described by the NEMD simulation. Furthermore, using boundary specularity is already a simplified approach to deal with phonon transport for those relatively small pores in nanoporous materials. As such, we cannot see a particular setup of boundary specularity in BTE that ensures consistency with NEMD. Therefore, we adopt the diffusely reflecting boundary for the pore edges to keep consistent with the literature [61–64].

3. Results

We investigate the behaviors of wave effect in periodic and aperiodic nanoporous graphene with different periods, lengths, and degrees of disorder. The thermal conductivities of periodic and aperiodic nanoporous graphene computed by NEMD and BTE are denoted by $\kappa_{\text{p,NEMD}}$, $\kappa_{\text{p,BTE}}$, $\kappa_{\text{ap,NEMD}}$ and $\kappa_{\text{ap,BTE}}$ in the following text. The results of the aperiodic nanoporous graphene presented in this work represent the averages of three independently generated configurations.

3.1. Period

We first investigate the wave effect in nanoporous graphene with different periods. Based on previous investigations, for graphene at 300 K, nearly 80% of thermal conductivity is contributed by the phonons with wavelengths below 2 nm [13]. Accordingly, we select 1.3, 1.7, 2.2, 2.6, 3.9, and 7.8 nm as typical periods, in which the dominant phonon wavelength is included. The total length of nanoporous graphene is fixed at 38 nm. For aperiodic configurations, the degree of disorder is set as the maximum (the definition of degree of disorder can be referred to Section 2.1). Namely, the pores are randomly shifted in a maximum space without overlapping.

Fig. 3 shows the $\kappa_{\text{p,NEMD}}$, $\kappa_{\text{p,BTE}}$, $\kappa_{\text{ap,NEMD}}$ and $\kappa_{\text{ap,BTE}}$ changing with periods. We first consider the NEMD results. As shown in Fig. 3a, the thermal conductivity of the periodic structure $\kappa_{\text{p,NEMD}}$ first decreases and then increases with the period and reaches a minimum at $p = 1.7$ nm. This phenomenon is usually attributed to the transition of coherent to incoherent phonon transport in periodic structures [43,65–67]. Similar to periodic cases, the thermal conductivity of the aperiodic structure $\kappa_{\text{ap,NEMD}}$, shown in Fig. 3b, also has a transition with the period. This is

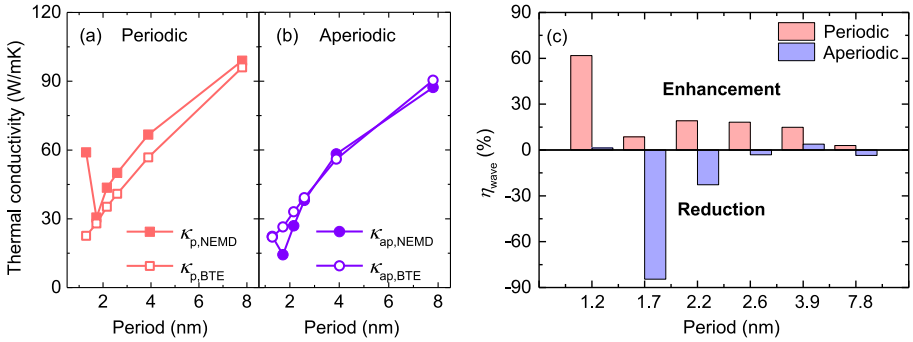

Fig. 3. The effect of the period on the wave effect contribution. (a) Thermal conductivities of periodic nanoporous graphene, (b) thermal conductivities of aperiodic nanoporous graphene, and (c) the corresponding wave effect contributions changing with the period. The length of all configurations is fixed at 38 nm. (A colour version of this figure can be viewed online.)

because, according to our setups, for very small periods, the space for randomly shifting the pores is limited by the small neck width and thus the degree of disorder is small.

We then consider the BTE results. For all the periods, $\kappa_{p,BTE}$ (see Fig. 3a) and $\kappa_{ap,BTE}$ (see Fig. 3b) are close and both increase moronically with the increasing period. This is because as the period increases, the corresponding boundary density reduces, resulting in reduced phonon-boundary scattering [20].

We finally look at the difference between the thermal conductivities obtained from NEMD and BTE. Fig. 3c shows the corresponding wave effect contributions η_{wave} that are quantified according to Eq. (1). For periodic structures, the wave effect contributions are positive for all periods. It reaches 60% at a period of 1.3 nm and then decreases in a non-monotonic manner. At the period of 2.2, 2.6, and 3.9 nm, the wave effect contribution can still reach 15%~20%. At the period of 7.8 nm, the wave effect contribution is only around 3%. For aperiodic structures, the wave effect contribution can be positive, negative, or nearly none. At the period of 1.7 nm, η_{wave} is around −84%. At the period of 2.2 nm, the absolute value of η_{wave} decreases to 22%. While for a period of 2.6, 3.9, and 7.8 nm, the absolute values of η_{wave} are only around 3%. As shown in Fig. 3c, for our studied systems, the wave effect in periodic structure enhances thermal transport compared to solely particle transport, while the wave effect in aperiodic structure generally reduces thermal transport compared to solely particle transport.

3.2. Length

We then investigate the influence of length on the wave effect. We consider the nanoporous graphene of periods 1.3, 1.7, and 7.8 nm with lengths from 38 to 325 nm. Similar to Section 3.1, for aperiodic configurations, the degree of disorder is set as the maximum.

Fig. 4 presents $\kappa_{p,NEMD}$, $\kappa_{p,BTE}$, $\kappa_{ap,NEMD}$ and $\kappa_{ap,BTE}$ changing with length. We first consider the NEMD results. For all the periods, the thermal conductivities of periodic configurations $\kappa_{p,NEMD}$ increase with the total length L. For aperiodic cases, the thermal conductivities $\kappa_{ap,NEMD}$ also gradually increase with the increasing length, but the increment is smaller than that of periodic ones. These results are consistent with previous studies [37,46].

We then consider the BTE results. For the period of 1.3 (Figs. 4a) and 1.7 nm (Fig. 4b), $\kappa_{p,BTE}$ and $\kappa_{ap,BTE}$ first increase with L and then saturate, while for the period of 7.8 nm (Fig. 4c), they still increase until 300 nm. These different behaviors also originate from decreasing boundary density with the increasing period. With a short period, phonons scatter frequently at pore edges and behave like diffuse transport. With a large period, some phonons with long MFPs are still not sufficiently scattered and behave like ballistic transport. Hence, the thermal conductivity is length-dependent.

Finally, we compare the NEMD and BTE calculated thermal conductivities. Fig. 5a and Fig. 5b present the corresponding wave effect contribution η_{wave} of periodic and aperiodic cases, respectively. For the periodic structure, the contributions of the wave effect are positive and increase with increasing length. As the length increases from 38 nm to around 325 nm, η_{wave} increase from 60% to 80% for the period of 1.3 nm, from 8% to 43% for the period of 1.7 nm and from 3% to 30% for the period of 7.8 nm. As for aperiodic structure, η_{wave} also increases with total length for the period of 1.3 nm and 1.7 nm. For 1.3 nm, the η_{wave} increase from 1% to 21%. For 1.7 nm, the η_{wave} increase from −85% to −40%. For 7.8 nm, the η_{wave} have nearly no changes and is close to 0.

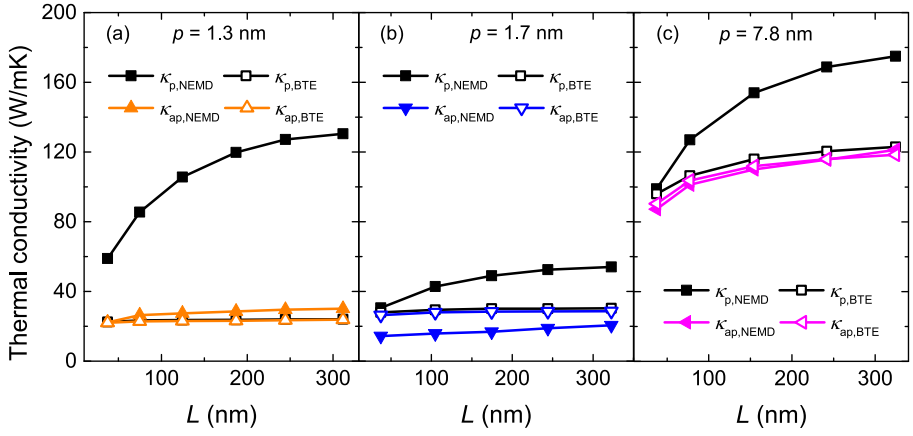

Fig. 4. Thermal conductivities of periodic and aperiodic nanoporous graphene changing with system length with a period of 1.3 nm (a), 1.7 nm (b) and 7.8 nm (c). (A colour version of this figure can be viewed online.)

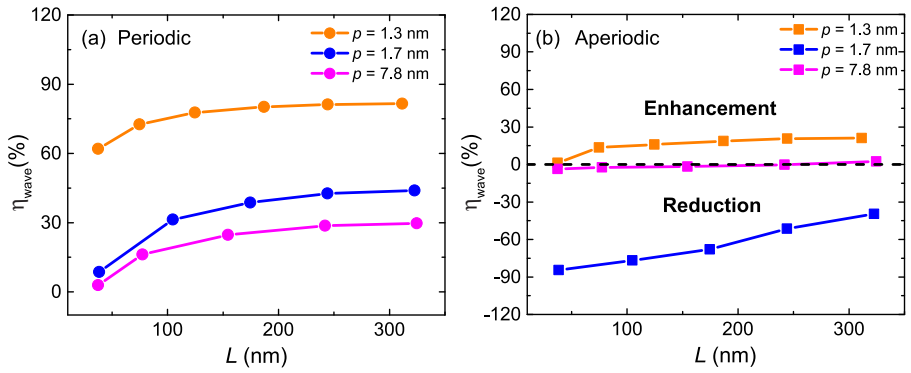

Fig. 5. The wave effect of periodic nanoporous graphene (a) and aperiodic nanoporous graphene (b) as a function of length. The "enhancement" and "reduction" denote that the dominant wave effect enhances and reduces the thermal conductivity compared to solely particle-like transport, respectively. (A colour version of this figure can be viewed online.)

3.3. Degree of disorder

In addition to the system period and length, the pore arrangement can also have a great impact on the thermal transport of nanoporous materials [20,47,68,69]. Here, we examine the influence of pore arrangement on the thermal conductivity and wave effect contribution by considering different degrees of disorder in the *x* and *y*-direction (δ_x, δ_y), which are along and perpendicular to the heat flux, respectively. It should be emphasized that in the results above, the degrees of disorder in aperiodic configurations are set as the maximum value. In this section, we consider different degrees of disorder. We generate three groups of aperiodic nanoporous graphene of period 7.8 nm with different degrees of disorder. Group I includes configurations only disordered in the *x*-direction, of which (δ_x, δ_y) is (5,0) and (10,0). Group II includes configurations only disordered in the *y*-direction with (δ_x, δ_y) of (0,2) and (0,5). Group III includes configurations disordered in both *x*, *y*-direction with (δ_x, δ_y) of (5,2) and (10,5). A larger value of δ_x or δ_y means that the shift of pores from the centers is larger and the configuration is more disordered.

Fig. 6 shows the thermal conductivities (Fig. 6a) and corresponding wave effect contributions (Fig. 6b) of the three groups. The schematic figures of configurations of group I, II, and III are presented at the top of Fig. 6. The BTE calculated thermal conductivities κ_{BTE} (hollow squares) of all three groups are close. Nevertheless, the NEMD simulated thermal conductivities κ_{NEMD} (filled squares) of three groups have a distinct difference. κ_{NEMD} of group I are higher than that of group II and III. Furthermore, the increasing degrees of disorder lead to lower thermal conductivities for group II and III, while the influence is less significant for group I. The trend of wave effect contribution is similar to the NEMD simulated thermal conductivity κ_{NEMD}. η_{wave} of group I are higher than that of group II and III. For group I, η_{wave} are around 25%. For group II and III, η_{wave} of aperiodic structures with a small and large degree of disorder in the *y*-direction are around 15% and 5%, respectively.

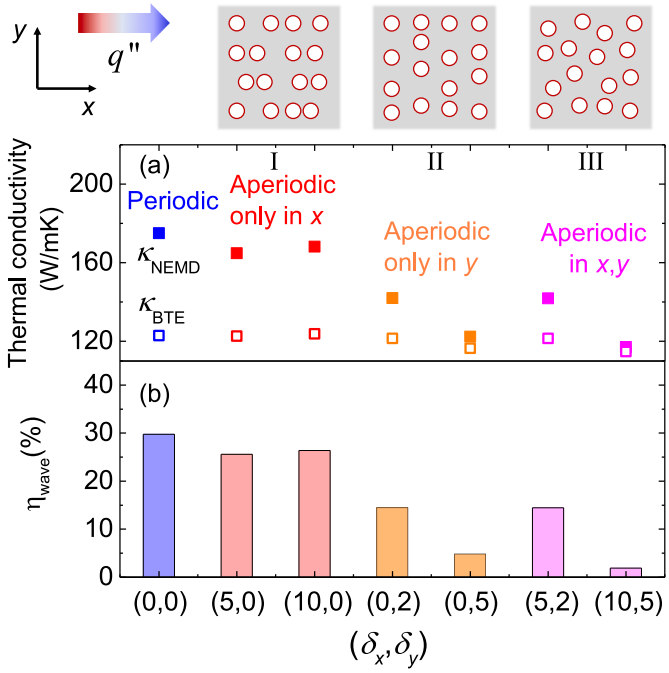

Fig. 6. The effect of the degree of disorder on the thermal conductivity (a) and wave effect contribution (b). Group I denotes configurations only disordered in the *x*-direction with (δ_x, δ_y) of (5,0) and (10,0). Group II denotes configurations only disordered in the *y*-direction with (δ_x, δ_y) of (0,2) and (0,5). Group III denotes configurations disordered in both *x*, *y*-direction with (δ_x, δ_y) of (5,2) and (10,5). The schematic figures of configurations of group I, II, and III are presented at the top. All the aperiodic configurations are of period 7.8 nm and length 325 nm. (A colour version of this figure can be viewed online.)

4. Discussion

We first discuss the overall behavior of wave effects in periodic and aperiodic nanoporous graphene. As seen from Figs. 3c and 5a, for the periodic structures, wave effect contributions to the overall thermal conductivity are positive for all the cases we study here. This indicates that the wave effect in periodic nanoporous graphene enhances the thermal conductivity compared to solely particle transport. BTE thus underestimates the thermal conductivity of periodic structures by omitting the coherent transport.

The wave transport in aperiodic structures is more complicated. As shown in Figs. 3 and 4, the thermal conductivities $\kappa_{ap,NEMD}$ are much lower than $\kappa_{p,NEMD}$, while the values of $\kappa_{p,BTE}$ and $\kappa_{ap,BTE}$ are very close. This means that the reduction of NEMD simulated thermal conductivity is due to the wave effect, e.g. phonon localization. Figs. 3c and 5b present the wave effect contributions of aperiodic nanoporous graphene that can be positive, negative, or none. The negative values of wave effect contribution provide direct evidence of reducing thermal conductivity by phonon localization. However, it is interesting to find that for some aperiodic structures, the wave effect contributions are positive. This reveals that besides the phonon localization that impedes the thermal transport, there also exists another wave effect of enhancing thermal transport. These diverse wave effects both originate from coherent transport but have different behaviors. As denoted in Fig. 5, after the competition of these diverse wave effects, the overall coherent transport may enhance or reduce the thermal conductivity compared to solely particle-based prediction. However, we should note that for the period 7.8 nm, the wave effect contributions close to zero do not

manifest that the wave effect is not important. On the contrary, the diverse wave effects are both strong, but they cancel each other and the final apparent results appear to have no wave effects, which would be an erroneous interpretation.

We then discuss the detailed behavior of wave effect changing with periods, lengths, and degrees of disorder. As for the period, the absolute values of η_{wave} of periodic and aperiodic structures are generally larger at smaller periods, as shown in Fig. 3. This is because when the period is small, wave interference is easier to occur and thus phonon coherent transport that enhances or impedes thermal transport is both strong.

Next, we discuss the impact of length on the thermal conductivity and wave effect contribution. As seen in Fig. 4, for periodic structures, the $\kappa_{p,BTE}$ and ($\kappa_{p,NEMD} - \kappa_{p,BTE}$) both increase with length. This means that the increase of thermal conductivity of periodic nanoporous graphene with length results from both the particle-based ballistic transport and wave-based coherent transport. In longer systems, the ballistic transport of phonons with long mean free paths leads to larger thermal conductivity. On the other hand, long-wavelength phonons can be excited in longer systems, which enhances the coherent transport and increase the thermal conductivity. For the period of 1.3 (Fig. 4a) and 1.7 nm (Fig. 4b), the particle-based ballistic transport is limited by frequent boundary scattering and most heat is carried by wave-based coherent transport. While for the period of 7.8 nm (Fig. 4c), both the particle-based ballistic transport and wave-based coherent transport contribute to the overall thermal conductivity. For aperiodic structures of period 1.3 and 1.7 nm, the wave effect contribution η_{wave} also gradually increase with the length. This is because the space for randomly shifting the pores is limited by the small neck width and thus the degree of disorder is very small. In these aperiodic structures, the wave effect that enhances thermal conductivity dominates over phonon localization that reduces thermal conductivity, so overall wave effects increase with the system length. For aperiodic structures of period 7.8 nm, as discussed before, the diverse wave effects cancel each other and thus η_{wave} do not increase with the length.

For aperiodic structures, as shown in Fig. 6, the wave effect contributions also vary with different degrees of disorder. η_{wave} of aperiodic structures with the disorder in the direction perpendicular to heat flux are smaller than that only in the direction parallel to heat flux, even the average shifted distance of the latter is larger. This means that the phonon wave transport is more sensitive to the disorder perpendicular to heat flux. This phenomenon is possibly attributed to the different thermal transport channels [19,70] caused by the disorder in the direction parallel or perpendicular to heat flux. The region between two rows of pores that aligns along the heat flux is usually denoted as a channel [19,70,71]. The formation of a channel in nanoporous materials is beneficial for phonon transport due to the lack of phonon-boundary scattering. The disorder in the direction parallel to heat flux does not influence the channels. However, the disorder in the direction perpendicular to heat flux may block the channels, thereby increasing the phonon-boundary scattering. In this case, the phase of phonons may not retain and the coherent transport may be destroyed. As such, the contribution of the wave effect is reduced.

As a final remark, we note that different phonon transport behaviors are originated from the broad-spectrum nature of phonons. A spectral-level decomposition of different phonon transport behaviors will provide more insights. However, the state-of-the-art spectral analysis method, such as spectral energy density analysis [51,72], mode decomposition [73,74], and wave packet simulation [75,76], still cannot achieve the mode-level decomposition of wave and particle transport. This could be a promising direction for future research.

5. Conclusion

In summary, we quantitatively study the diverse wave effects that enhance or reduce the thermal transport of nanoporous graphene. These wave effects are rigorously distinguished and quantified by comparing the thermal conductivities from NEMD simulation and mode-resolved phonon BTE calculation. We find that for periodic nanoporous graphene, the phonon wave effect has a positive contribution to the total thermal conductivity. For aperiodic configurations, the wave effect contribution can be positive, negative, or negligible, as a result of the competition of diverse wave effects. The overall contributions of wave effects to the thermal conductivity of nanoporous graphene changing with periods, lengths, and degrees of the disorder are also investigated in detail. In periodic and aperiodic structures, the absolute values of wave effect contribution non-monotonically decrease with periods and monotonically increases with lengths. For aperiodic structures, the disorder perpendicular to the heat flux direction leads to lower thermal conductivity than the disorder aligning along with the heat flux. With an increasing degree of disorder, the total wave effect contribution is smaller. Our work provides new insights into thermal transport in nanoporous structures and theoretical guidance to the further manipulation of thermoelectric performance.

CRediT authorship contribution statement

Han Wei: Methodology, Investigation, Formal analysis, Visualization, Writing – original draft. **Yue Hu:** Software, Validation, Data curation, Writing – review & editing. **Hua Bao:** Conceptualization, Writing – review & editing, Funding acquisition, Supervision. **Xiulin Ruan:** Conceptualization, Writing – review & editing, Supervision.

Declaration of competing interest

The authors declare that they have no known competing financial interests or personal relationships that could have appeared to influence the work reported in this paper.

Acknowledgment

H.B. acknowledges the support provided by the National Natural Science Foundation of China (No. 52122606) and H.W. acknowledges Zhiyuan Honor Ph.D. fellowship program of Shanghai Jiao Tong University. The computations in this paper were run on the π 2.0 cluster supported by the Center for High Performance Computing at Shanghai Jiao Tong University.

Appendix Reconstruction of phonon cumulative MFP distribution from NEMD

We reconstruct the cumulative phonon MFP distribution from length-dependent thermal conductivity computed by NEMD. The length-dependent thermal conductivity $\kappa(L)$ is related to the cumulative phonon MFP distribution $F(\Lambda_\omega)$ through the suppression function $S(\eta)$ by Ref. [57]:

$$\kappa(L) = \int_0^\infty S(\eta) f(\Lambda_\omega) \mathrm{d}\Lambda_\omega = \int_0^\infty \frac{1}{L} K(\eta) F(\Lambda_\omega) \mathrm{d}\Lambda_\omega, \tag{2}$$

where $\eta = \frac{\Lambda_\omega}{L}$ is the ratio of the spectral MFP to the system length. $K(\eta) = -\mathrm{d}S/\mathrm{d}\eta$ is the kernel function, and $f(\Lambda_\omega)$ is the differential phonon MFP distribution. $F(\Lambda_\omega)$ is related to $f(\Lambda_\omega)$ by $F(\Lambda_\omega) = \int_0^{\Lambda_\omega} f(\Lambda') d\Lambda'$. The suppression function describes the suppression of thermal conductivity as a function

of system length due to the confinement of ballistic phonons [77]. It incorporates the information of geometry and boundary conditions (the distribution of heat sources) of the system [56]. The MFP distribution incorporates the material information of the system [56,57]. Once the length-dependent thermal conductivity and the suppression function are provided, the MFP distribution can be reconstructed based on Eq. (2).

We take the cross-plane thermal transport as the model system (as shown in the inserted figure in Fig. 2a.) to reconstruct the MFP distribution of graphene. NEMD simulations with the Langevin thermostat are used to compute the thermal conductivities of graphene at different lengths, which are shown in Fig. 2a. The suppression function can be obtained by solving BTE analytically for a simple geometry or numerically for more complex geometries [78]. When obtaining the suppression function [57], the most important prerequisite is to ensure that the system of measuring the length-dependent thermal conductivity is equivalent to that of calculating the suppression function. It has been proved that for the cross-plane thermal transport in pristine material, the NEMD simulation with Langevin thermostat and BTE calculation with thermalizing boundary conditions are equivalent [50]. Accordingly, we compute the suppression function of cross-plane thermal transport by BTE with thermalizing boundary conditions. The details of reconstructing the MFP distribution are as follows.

The suppression function of cross-plane thermal transport of 2D phase space [77] (since graphene is a 2D material) is solved by a gray-body BTE calculation with thermalizing boundary conditions. If we assume that the suppression function only depends on the geometry and boundary conditions, the same suppression function is also applicable to the gray medium where the MFPs of all phonons are the same [79]. Namely, the suppression function can be calculated from the gray-body BTE. In practice, the above assumption is not strictly rigorous. Nevertheless, it has been proven to work well in previous studies [79,80]. Therefore, we still use this assumption here. Under this assumption, η in Eq. (2) is just the Knudsen number Kn. We calculate several discrete values of suppression function at different Knudsen numbers by gray-body BTE and then fit them into a function $S(Kn) = 1 - \frac{A}{1+e^{a-b\ \ln(Kn)}}$. The fitting parameters A, a, and b is taken as 0.999, −0.491, and 1.002, respectively. Fig. 7a shows the calculated and fitted suppression function, which are denoted by pink circles and a black line, respectively. It is seen that the fitted suppression function is quite close to the calculated one. The kernel function K is obtained by taking the derivative of suppression function S as $K(Kn) = -\frac{dS}{dKn} = \frac{Abe^{a-b\ \ln(Kn)}}{(1+e^{a-b\ \ln(Kn)})^2} \cdot \frac{1}{Kn}$, which is shown in Fig. 7a using a red dashed line. After obtaining the length-dependent thermal conductivities and suppression function, we follow the method introduced in Ref. [57] to discretize the integral in Eq. (2) using Gaussian quadrature and obtain the cumulative MFP distribution by convex optimization [57]. Fig. 7b shows the obtained thermal conductivity accumulation (normalized) as a function of Kn. The reconstructed MFP distribution is then used as the input of mode-resolved BTE calculation.

We note that another approach to obtaining the phonon properties of the material is to extract from the interatomic potential used in MD by the anharmonic lattice dynamics (LD) approach [81]. However, there are usually some discrepancies between the results from LD-BTE and MD methods because if lattice dynamics is used to extract phonon properties, BTE includes less phonon scattering than MD [82]. To avoid such a discrepancy, in the present work, we did not use lattice dynamics to extract phonon properties. Instead, we reconstruct the intrinsic cumulative MFP distribution from NEMD simulations of the length-dependent thermal conductivities. This approach is easier to implement and can obtain the accurate cumulative MFP distribution inherently including all orders of scattering processes. Through this approach, the MFP distributions of materials have been successfully reconstructed from various nanostructures, like the membrane [83], nanowire [77], nanoribbon [77], and grating [79].

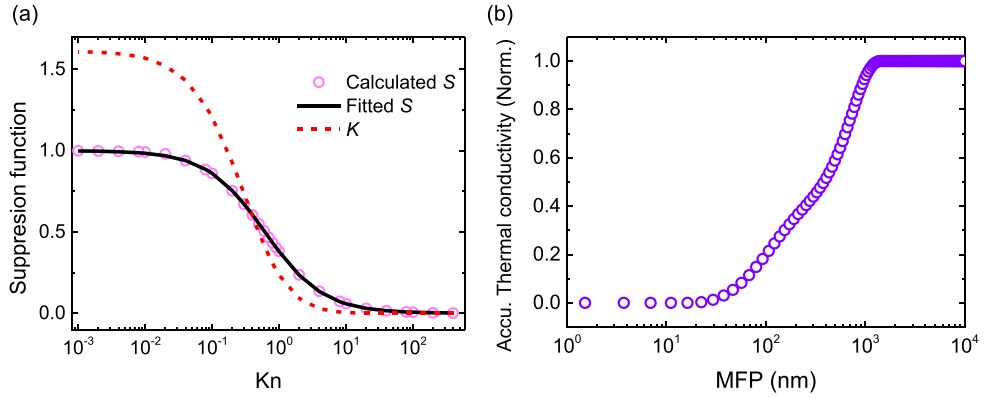

Fig. 7. Reconstruction of intrinsic MFP distribution of graphene. (a) The calculated suppression function (pink circles), fitted suppression function (black solid line) and kernel function (red dashed line). (c) Reconstructed thermal conductivity accumulation (normalized) as a function of phonon MFP.

Appendix A. Supplementary data

Supplementary data to this article can be found online at https://doi.org/10.1016/j.carbon.2022.06.011.

References

[1] K.S. Novoselov, A.K. Geim, S.V. Morozov, D.-e. Jiang, Y. Zhang, S.V. Dubonos, I. V. Grigorieva, A.A. Firsov, Electric field effect in atomically thin carbon films, science 306 (5696) (2004) 666–669.
[2] R.R. Nair, P. Blake, A.N. Grigorenko, K.S. Novoselov, T.J. Booth, T. Stauber, N.M. R. Peres, A.K. Geim, Fine structure constant defines visual transparency of graphene, Science 320 (5881) (2008), 1308-1308.
[3] M.-F. Yu, O. Lourie, M.J. Dyer, K. Moloni, T.F. Kelly, R.S. Ruoff, Strength and breaking mechanism of multiwalled carbon nanotubes under tensile load, Science 287 (5453) (2000) 637–640.
[4] D.G. Cahill, W.K. Ford, K.E. Goodson, G.D. Mahan, A. Majumdar, H.J. Maris, R. Merlin, S.R. Phillpot, Nanoscale thermal transport, J. Appl. Phys. 93 (2) (2003) 793–818.
[5] S. Volz, J. Shiomi, M. Nomura, K. Miyazaki, Heat conduction in nanostructured materials, J. Therm. Sci. Technol. 11 (1) (2016). JTST0001-JTST0001.
[6] H. Bao, J. Chen, X. Gu, B. Cao, A review of simulation methods in micro/nanoscale heat conduction, ES Energy & Environment 1 (34) (2018) 16–55.
[7] M. Hu, Z. Yang, Perspective on multi-scale simulation of thermal transport in solids and interfaces, Phys. Chem. Chem. Phys. 23 (3) (2020) 1785–1801.
[8] W.J. Evans, L. Hu, P. Keblinski, Thermal conductivity of graphene ribbons from equilibrium molecular dynamics: effect of ribbon width, edge roughness, and hydrogen termination, Appl. Phys. Lett. 96 (20) (2010), 203112.
[9] G. Xie, Y. Shen, Size and edge roughness dependence of thermal conductivity for vacancy-defective graphene ribbons, Phys. Chem. Chem. Phys. 17 (14) (2015) 8822–8827.

[10] Y. Wang, B. Qiu, X. Ruan, Edge effect on thermal transport in graphene nanoribbons: a phonon localization mechanism beyond edge roughness scattering, Appl. Phys. Lett. 101 (1) (2012), 013101.
[11] C.A. Polanco, L. Lindsay, Ab initio phonon point defect scattering and thermal transport in graphene, Physical Review. B, Covering Condensed Matter and Materials Physics; College Park 97 (1) (2018).
[12] S. Hu, J. Chen, N. Yang, B. Li, Thermal transport in graphene with defect and doping: phonon modes analysis, Carbon 116 (2017) 139–144.
[13] T. Feng, X. Ruan, Z. Ye, B. Cao, Spectral phonon mean free path and thermal conductivity accumulation in defected graphene: the effects of defect type and concentration, Phys. Rev. B 91 (22) (2015), 224301.
[14] M. Li, T. Deng, B. Zheng, Y. Zhang, Y. Liao, H. Zhou, Effect of defects on the mechanical and thermal properties of graphene, Nanomaterials 9 (3) (2019) 347.
[15] B. Mortazavi, S. Ahzi, Thermal conductivity and tensile response of defective graphene: a molecular dynamics study, Carbon 63 (2013) 460–470.
[16] Y.P. Bliokh, V. Freilikher, S. Savel'ev, F. Nori, Transport and localization in periodic and disordered graphene superlattices, Phys. Rev. B 79 (7) (2009), 075123.
[17] I.M. Felix, L.F.C. Pereira, Suppression of coherent thermal transport in quasiperiodic graphene-hBN superlattice ribbons, Carbon 160 (2020) 335–341.
[18] X. Mu, T. Zhang, D.B. Go, T. Luo, Coherent and incoherent phonon thermal transport in isotopically modified graphene superlattices, Carbon 83 (2015) 208–216.
[19] H. Wei, H. Bao, X. Ruan, Genetic algorithm-driven discovery of unexpected thermal conductivity enhancement by disorder, Nano Energy 71 (2020), 104619.
[20] T. Feng, X. Ruan, Ultra-low thermal conductivity in graphene nanomesh, Carbon 101 (2016) 107–113.
[21] J. Oh, H. Yoo, J. Choi, J.Y. Kim, D.S. Lee, M.J. Kim, J.-C. Lee, W.N. Kim, J. C. Grossman, J.H. Park, S.-S. Lee, H. Kim, J.G. Son, Significantly reduced thermal conductivity and enhanced thermoelectric properties of single- and bi-layer graphene nanomeshes with sub-10 nm neck-width, Nano Energy 35 (2017) 26–35.
[22] J. Bai, X. Zhong, S. Jiang, Y. Huang, X. Duan, Graphene nanomesh, Nat. Nanotechnol. 5 (3) (2010) 190–194.
[23] A.A. Balandin, D.L. Nika, Phononics in low-dimensional materials, Mater. Today 15 (6) (2012) 266–275.
[24] M. Maldovan, Sound and heat revolutions in phononics, Nature 503 (7475) (2013) 209–217.
[25] M. Maldovan, Phonon wave interference and thermal bandgap materials, Nat. Mater. 14 (7) (2015) 667–674.
[26] P. Pichanusakorn, P. Bandaru, Nanostructured thermoelectrics, Mater. Sci. Eng. R Rep. 67 (2) (2010) 19–63.
[27] G. Chen, M.S. Dresselhaus, G. Dresselhaus, J.P. Fleurial, T. Caillat, Recent developments in thermoelectric materials, Int. Mater. Rev. 48 (1) (2003) 45–66.
[28] J.R. Szczech, J.M. Higgins, S. Jin, Enhancement of the thermoelectric properties in nanoscale and nanostructured materials, J. Mater. Chem. 21 (12) (2011) 4037–4055.
[29] Q.-Y. Li, Q. Hao, T. Zhu, M. Zebarjadi, K. Takahashi, Nanostructured and heterostructured 2D materials for thermoelectrics, Engineered Science 13 (2021) 24–50.
[30] J.-H. Lee, G.A. Galli, J.C. Grossman, Nanoporous Si as an efficient thermoelectric material, Nano Lett. 8 (11) (2008) 3750–3754.
[31] P. Dollfus, V.H. Nguyen, J. Saint-Martin, Thermoelectric effects in graphene nanostructures, J. Phys. Condens. Matter 27 (13) (2015), 133204.
[32] J.-K. Yu, Reduction of thermal conductivity in phononic nanomesh structures, Nat. Nanotechnol. 5 (10) (2010) 718–721.
[33] S. Alaie, D.F. Goettler, M. Su, Z.C. Leseman, C.M. Reinke, I. El-Kady, Thermal transport in phononic crystals and the observation of coherent phonon scattering at room temperature, Nat. Commun. 6 (1) (2015) 7228.
[34] Z. Xiong, X. Wang, K.H.K. Lee, X. Zhan, Y. Chen, J. Tang, Thermal transport in supported graphene nanomesh, ACS Appl. Mater. Interfaces 10 (11) (2018) 9211–9215.
[35] M. Yarifard, J. Davoodi, H. Rafii-Tabar, In-plane thermal conductivity of graphene nanomesh: a molecular dynamics study, Comput. Mater. Sci. 111 (2016) 247–251.
[36] L. Cui, G. Wei, Z. Li, X. Du, Thermal transport in graphene nanomesh: unraveling the role of brillouin zone folding, phonon localization and phonon confinement, Int. J. Heat Mass Tran. 165 (2021), 120685.
[37] S. Hu, Z. Zhang, P. Jiang, J. Chen, S. Volz, M. Nomura, B. Li, Randomness-induced phonon localization in graphene heat conduction, J. Phys. Chem. Lett. 9 (14) (2018) 3959–3968.
[38] S.R. Nagel, G.S. Grest, A. Rahman, Phonon localization and anharmonicity in model glasses, Phys. Rev. Lett. 53 (4) (1984) 368–371.
[39] S.G. Cloutier, R.S. Guico, J.M. Xu, Phonon localization in periodic uniaxially nanostructured silicon, Appl. Phys. Lett. 87 (22) (2005), 222104.
[40] A. Kundu, A. Chaudhuri, D. Roy, A. Dhar, J.L. Lebowitz, H. Spohn, Heat conduction and phonon localization in disordered harmonic crystals, EPL 90 (4) (2010), 40001.
[41] T. Juntunen, O. Vänskä, I. Tittonen, Anderson localization quenches thermal transport in aperiodic superlattices, Phys. Rev. Lett. 122 (10) (2019), 105901.
[42] R. Hu, S. Iwamoto, L. Feng, S. Ju, S. Hu, M. Ohnishi, N. Nagai, K. Hirakawa, J. Shiomi, Machine-Learning-optimized aperiodic superlattice minimizes coherent phonon heat conduction, Phys. Rev. X 10 (2) (2020), 021050.
[43] P. Roy Chowdhury, C. Reynolds, A. Garrett, T. Feng, S.P. Adiga, X. Ruan, Machine learning maximized Anderson localization of phonons in aperiodic superlattices, Nano Energy 69 (2020), 104428.
[44] S. Hu, Z. Zhang, P. Jiang, W. Ren, C. Yu, J. Shiomi, J. Chen, Disorder limits the coherent phonon transport in two-dimensional phononic crystal structures, Nanoscale 11 (24) (2019) 11839–11846.
[45] P.E. Hopkins, C.M. Reinke, M.F. Su, R.H. Olsson, E.A. Shaner, Z.C. Leseman, J. R. Serrano, L.M. Phinney, I. El-Kady, Reduction in the thermal conductivity of single crystalline silicon by phononic crystal patterning, Nano Lett. 11 (1) (2011) 107–112.
[46] Y. Wang, H. Huang, X. Ruan, Decomposition of coherent and incoherent phonon conduction in superlattices and random multilayers, Phys. Rev. B 90 (16) (2014), 165406.
[47] J. Maire, R. Anufriev, R. Yanagisawa, A. Ramiere, S. Volz, M. Nomura, Heat conduction tuning by wave nature of phonons, Sci. Adv. 3 (8) (2017), e1700027.
[48] D. Ma, A. Arora, S. Deng, G. Xie, J. Shiomi, N. Yang, Quantifying phonon particle and wave transport in silicon nanophononic metamaterial with cross junction, Materials Today Physics 8 (2019) 56–61.
[49] D. Chakraborty, H. Karamitaheri, L. de Sousa Oliveira, N. Neophytou, Effect of wave versus particle phonon nature in thermal transport through nanostructures, Comput. Mater. Sci. 180 (2020), 109712.
[50] Y. Hu, T. Feng, X. Gu, Z. Fan, X. Wang, M. Lundstrom, S.S. Shrestha, H. Bao, Unification of nonequilibrium molecular dynamics and the mode-resolved phonon Boltzmann equation for thermal transport simulations, Phys. Rev. B 101 (15) (2020), 155308.
[51] J.A. Thomas, J.E. Turney, R.M. Iutzi, C.H. Amon, A.J.H. McGaughey, Predicting phonon dispersion relations and lifetimes from the spectral energy density, Phys. Rev. B 81 (8) (2010), 081411.
[52] J.Y. Murthy, S.R. Mathur, Computation of sub-micron thermal transport using an unstructured finite volume method, J. Heat Tran. 124 (6) (2002) 1176–1181.
[53] S.V.J. Narumanchi, J.Y. Murthy, C.H. Amon, Submicron heat transport model in silicon accounting for phonon dispersion and polarization, J. Heat Tran. 126 (6) (2004) 946–955.
[54] F. Yang, C. Dames, Mean free path spectra as a tool to understand thermal conductivity in bulk and nanostructures, Phys. Rev. B 87 (3) (2013), 035437.
[55] G. Romano, J.C. Grossman, Heat conduction in nanostructured materials predicted by phonon bulk mean free path distribution, J. Heat Tran. 137 (7) (2015), 071302.
[56] K.T. Regner, J.P. Freedman, J.A. Malen, Advances in studying phonon mean free path dependent contributions to thermal conductivity, Nanoscale Microscale Thermophys. Eng. 19 (3) (2015) 183–205.
[57] A.J. Minnich, Determining phonon mean free paths from observations of quasiballistic thermal transport, Phys. Rev. Lett. 109 (20) (2012), 205901.
[58] Z. Li, S. Xiong, C. Sievers, Y. Hu, Z. Fan, N. Wei, H. Bao, S. Chen, D. Donadio, T. Ala-Nissila, Influence of thermostatting on nonequilibrium molecular dynamics simulations of heat conduction in solids, J. Chem. Phys. 151 (23) (2019), 234105.
[59] S. Plimpton, Fast parallel algorithms for short-range molecular dynamics, J. Comput. Phys. 117 (1) (1995) 1–19.
[60] L. Lindsay, D.A. Broido, Optimized Tersoff and Brenner empirical potential parameters for lattice dynamics and phonon thermal transport in carbon nanotubes and graphene, Phys. Rev. B 81 (20) (2010), 205441.
[61] Z. Yu, L. Ferrer-Argemi, J. Lee, Investigation of thermal conduction in symmetric and asymmetric nanoporous structures, J. Appl. Phys. 122 (24) (2017), 244305.
[62] N.K. Ravichandran, A.J. Minnich, Coherent and incoherent thermal transport in nanomeshes, Phys. Rev. B 89 (20) (2014), 205432.
[63] R. Yang, G. Chen, Thermal conductivity modeling of periodic two-dimensional nanocomposites, Phys. Rev. B 69 (19) (2004), 195316.
[64] G. Romano, A.M. Kolpak, J. Carrete, D. Broido, Parameter-free model to estimate thermal conductivity in nanostructured materials, Phys. Rev. B 100 (4) (2019), 045310.
[65] M.V. Simkin, G.D. Mahan, Minimum thermal conductivity of superlattices, Phys. Rev. Lett. 84 (5) (2000) 927–930.
[66] J. Ravichandran, A.K. Yadav, R. Cheaito, P.B. Rossen, A. Soukiassian, S.J. Suresha, J.C. Duda, B.M. Foley, C.-H. Lee, Y. Zhu, A.W. Lichtenberger, J.E. Moore, D. A. Muller, D.G. Schlom, P.E. Hopkins, A. Majumdar, R. Ramesh, M.A. Zurbuchen, Crossover from incoherent to coherent phonon scattering in epitaxial oxide superlattices, Nat. Mater. 13 (2) (2014) 168–172.
[67] G. Xie, D. Ding, G. Zhang, Phonon coherence and its effect on thermal conductivity of nanostructures, Adv. Phys. X 3 (1) (2018), 1480417.
[68] G. Romano, J.C. Grossman, Phonon bottleneck identification in disordered nanoporous materials, Phys. Rev. B 96 (11) (2017), 115425.
[69] M.R. Wagner, B. Graczykowski, J.S. Reparaz, A. El Sachat, M. Sledzinska, F. Alzina, C.M. Sotomayor Torres, Two-dimensional phononic crystals: disorder matters, Nano Lett. 16 (9) (2016) 5661–5668.
[70] H. Wei, H. Bao, X. Ruan, Machine learning prediction of thermal transport in porous media with physics-based descriptors, Int. J. Heat Mass Tran. 160 (2020), 120176.
[71] B.-Y. Cao, W.-J. Yao, Z.-Q. Ye, Networked nanoconstrictions: an effective route to tuning the thermal transport properties of graphene, Carbon 96 (2016) 711–719.
[72] J.M. Larkin, J.E. Turney, A.D. Massicotte, C.H. Amon, A.J.H. McGaughey, Comparison and evaluation of spectral energy methods for predicting phonon properties, J. Comput. Theor. Nanosci. 11 (1) (2014) 249–256.
[73] Y. Zhou, M. Hu, Erratum: quantitatively analyzing phonon spectral contribution of thermal conductivity based on nonequilibrium molecular dynamics simulations. II. From time Fourier transform [Phys. Rev. B 92, 195205 (2015)], Phys. Rev. B 93 (3) (2016), 039901.
[74] Y. Zhou, X. Zhang, M. Hu, Quantitatively analyzing phonon spectral contribution of thermal conductivity based on nonequilibrium molecular dynamics simulations. I. From space Fourier transform, Phys. Rev. B 92 (19) (2015), 195204.

[75] P.K. Schelling, S.R. Phillpot, P. Keblinski, Phonon wave-packet dynamics at semiconductor interfaces by molecular-dynamics simulation, Appl. Phys. Lett. 80 (14) (2002) 2484–2486.
[76] C. Shao, Q. Rong, M. Hu, H. Bao, Probing phonon–surface interaction by wave-packet simulation: effect of roughness and morphology, J. Appl. Phys. 122 (15) (2017), 155104.
[77] H. Zhang, C. Hua, D. Ding, A.J. Minnich, Length dependent thermal conductivity measurements yield phonon mean free path spectra in nanostructures, Sci. Rep. 5 (1) (2015) 9121.
[78] C. Hua, A.J. Minnich, Semi-analytical solution to the frequency-dependent Boltzmann transport equation for cross-plane heat conduction in thin films, J. Appl. Phys. 117 (17) (2015), 175306.
[79] L. Zeng, K.C. Collins, Y. Hu, M.N. Luckyanova, A.A. Maznev, S. Huberman, V. Chiloyan, J. Zhou, X. Huang, K.A. Nelson, G. Chen, Measuring phonon mean free path distributions by probing quasiballistic phonon transport in grating nanostructures, Sci. Rep. 5 (1) (2015), 17131.
[80] K.C. Collins, A.A. Maznev, Z. Tian, K. Esfarjani, K.A. Nelson, G. Chen, Non-diffusive relaxation of a transient thermal grating analyzed with the Boltzmann transport equation, J. Appl. Phys. 114 (10) (2013), 104302.
[81] D.A. Broido, M. Malorny, G. Birner, N. Mingo, D.A. Stewart, Intrinsic lattice thermal conductivity of semiconductors from first principles, Appl. Phys. Lett. 91 (23) (2007), 231922.
[82] X. Gu, Z. Fan, H. Bao, Thermal conductivity prediction by atomistic simulation methods: recent advances and detailed comparison, J. Appl. Phys. 130 (21) (2021), 210902.
[83] J. Cuffe, J.K. Eliason, A.A. Maznev, K.C. Collins, J.A. Johnson, A. Shchepetov, M. Prunnila, J. Ahopelto, C.M. Sotomayor Torres, G. Chen, K.A. Nelson, Reconstructing phonon mean-free-path contributions to thermal conductivity using nanoscale membranes, Phys. Rev. B 91 (24) (2015), 245423.